An isotropic damage model based on fracture mechanics for concrete

Mao Kurumatani [a,*], Kenjiro Terada [b], Junji Kato [c], Takashi Kyoya [c], Kazuo Kashiyama [d]

[a] Department of Urban and Civil Engineering, Ibaraki University, 4-12-1 Nakanarusawa, Hitachi, Ibaraki 316-8511, Japan
[b] International Research Institute of Disaster Science, Tohoku University, 468-1 Aza-Aoba, Aramaki, Aoba, Sendai 980-0845, Japan
[c] Department of Civil Engineering, Tohoku University, 6-6-06 Aza-Aoba, Aramaki, Aoba, Sendai 980-8579, Japan
[d] Department of Civil and Environmental Engineering, Chuo University, 1-13-27 Kasuga, Bunkyo-ku, Tokyo 112-8551, Japan

A R T I C L E   I N F O

A B S T R A C T

This paper presents an isotropic damage model for quasi-brittle materials and demonstrates its performance in crack propagation analysis for concrete. The suggested damage model is based on fracture mechanics for concrete in terms of the fracture energy and is therefore capable of simulating strain-softening behavior without mesh-size dependency. After the cohesive crack model is incorporated into a damage model in a 1D setting, the 1D model is extended to multi-dimensional problems by means of the equivalent strain of the modified von-Mises model. Several numerical examples are presented to examine the fundamental characteristics of the proposed damage model. In particular, we demonstrate that finite element solutions with the damage model are independent of mesh size and that the energy balance evaluated for the fracture process in a three-point bending test for a specimen with a single-edge notch is consistent with the fracture energy. A benchmark test for a mixed-mode fracture is also conducted to demonstrate the performance of the proposed damage model.

© 2016 Elsevier Ltd. All rights reserved.

1. Introduction

Materials such as concrete and ground/bedrock are not completely brittle materials, as they exhibit quasi-brittle fracture behavior, which results in failure with strain-softening. To reproduce the fracture behavior of such quasi-brittle materials efficiently and accurately, a considerable number of studies have been made on the developments of discretization methods and constitutive models, which still remain matter for debate.

Numerical techniques for fracture analysis with the finite element method (FEM) can roughly be classified into two groups. One is a class of constitutive models that represent strain-softening behavior associated with fracture, such as the smeared crack model and the damage model, whereas the other is a class of methods that incorporate discontinuous displacement fields into finite element (FE) approximations. In recent years, the latter class has been studied actively in the field of computational mechanics. It includes, for example, the embedded finite element method [1], which incorporates a discontinuous incompatible mode into a shape function in the FEM, the extended finite element method (X-FEM) [2] and the finite cover method (FCM) [3], both of which are based on the method of partition-of-unity (PU). The performances of these methods to capture arbitrary discontinuities independently of FE mesh and to evaluate strain-softening behavior have also been

---

* Corresponding author. Tel.: +81 294 38 5162; fax: +81 294 38 5268.
  E-mail address: mao.kurumatani.jp@vc.ibaraki.ac.jp (M. Kurumatani).

Nomenclature

σ	1D Cauchy stress
ε	1D small strain
E	Young's modulus
D	scalar damage variable ($0 \leqslant D \leqslant 1$)
f	1D cohesive force
w	1D crack opening displacement
A, B	unknown material parameters
f_t	uniaxial tensile strength
G_f	fracture energy
ε_0	damage initiation strain $\varepsilon_0 = f_t/E$
h	element length in 1D
h_e	representative element length in 2D or 3D
ϵ	1D maximum strain in the deformation history
α, β	material parameters in other references
ε_{eq}	equivalent strain defined as the modified von-Mises criterion
v	Poisson's ratio
k	ratio of tensile and compressive strength
$\boldsymbol{\varepsilon}$	small strain tensor
$\boldsymbol{e}$	deviatoric strain tensor
I_1	first invariant of strain tensor $\boldsymbol{\varepsilon}$
J_2	second invariant of deviatoric strain tensor $\boldsymbol{e}$
$\boldsymbol{\sigma}$	Cauchy stress tensor
$\boldsymbol{c}$	elastic modulus tensor
κ	maximum equivalent strain in the deformation history
A_e	area of 2D elements
V_e	volume of 3D elements
$\boldsymbol{C}$	material Jacobian
a_1, a_2	coefficients in Eq. (34)
G_F	apparent fracture energy estimated from numerical analyses

presented [4,5]. Although these methods are better suited for representing discontinuous displacements with high accuracy, the tracing of crack geometries seems to make it difficult to apply these methods to problems in which multiple cracks occur and interact with each other, or to 3D problems.

On the other hand, the former methods, which replace cracking and fracturing by material behavior characterized by appropriate constitutive relations, have been studied for a long time because of their good compatibility with the FEM. One of the representative methods for concrete is the crack band model [6], which expresses strain-softening behavior using tensile strength, fracture energy, and damage region width as parameters. The rotating crack model [7], which expresses crack nucleation/propagation and resulting softening behavior with the principal stress and its direction, is also one of the most fundamental models, and is capable of reproducing the anisotropy in crack formation. It is, however, known that these methods based on continuum mechanics often cause uncalled-for problems such as stress locking, depending on the FE mesh or crack geometry [7,8].

In the rotating crack model, the strain tensor is decomposed into elastic and inelastic parts to represent the strain-softening behavior. In contrast, in damage models, the strain-softening behavior is expressed by multiplying damage variables that represent the degree of mechanical degradation by elastic constants, without introduction of inelastic strains. Representative examples of these models include the isotropic damage model, in which damage variables are expressed as scalar-valued functions, and the anisotropic model based on the microplane model [9]. Although these models do not directly describe discontinuous displacements, they have proven to be effective in accurately reproducing the experimental results of concrete crack behavior [10,11]. In the damage evolution laws, however, several parameters irrespective of material responses have to be set to determine the functional form to represent strain-softening [12–14].

It is also known that incorporating a rotating crack model or a damage model into the FEM to analyze the strain-softening behavior entails the dependency of analysis results on element type or element size [15]. The so-called nonlocal models such as the integral average model [16] and the gradient model [17] are known to be common techniques to overcome this problem, namely, the lack of mesh-objectivity. Although applying these techniques enable us to reduce mesh dependency of analysis results to some extent, the determination of an integral radius in the nonlocal models or a gradient parameter in the gradient models is an additional task. It is indeed pointed out that the physical meanings of these parameters are ambiguous [18,19].

Several studies have also been made on introducing fracture mechanics model, which is called cohesive crack or cohesive zone model, into the finite element analysis for crack propagation. Hillerborg et al. [20] have proposed the energy balance approach as one of the cohesive model based on fracture mechanics for concrete in terms of fracture energy. In the cohesive model, cohesive tractions are assumed to act between crack surfaces to represent a fracture process zone in concrete. To simulate arbitrary propagating cracks in concrete using finite elements, the cohesive model has recently been incorporated with the PU-based FEM; see for example the X-FEM [21], PUFEM [22], FCM [23] and other related methods [24,25]. However, little attention has been paid to the combination of the cohesive model with the methods which replace the cracking by the degradation of stiffness represented by a continuum damage model, because the cohesive model is generally applied on the crack surfaces where cohesive tractions are transferred.

In this context, the purpose of this study is to propose an isotropic damage model based on fracture mechanics, which represents strain-softening behavior associated with cracking, without introducing the above-mentioned conventional nonlocal models. In order to verify the validity and effectiveness of the proposed model, we solve representative example problems of crack propagation in concrete. Section 2 starts with the formulation of the 1D damage model, which incorporates the well-known fracture mechanics model based on energy balance [20]. Then, we extend the model to multi-dimensional problems by using the equivalent strain of the modified von-Mises model [27]. In Section 3, verification is conducted to demonstrate the promise and capability of the proposed model for evaluating energy balance in deformation/fracture processes with high accuracy and without depending on element type and size. A benchmark problem involving mixed-mode fracture is also solved in Section 4 to demonstrate the ability of the proposed model in reproducing the corresponding experimental result.

2. Formulation of damage model based on fracture mechanics

The formulation of the proposed isotropic damage model is presented in this section. After incorporating the cohesive crack model into the 1D damage model within the framework of fracture mechanics, we extend the derived 1D model to multi-dimensional problems using the equivalent strain of the modified von-Mises model [27].

2.1. Formulation in 1D problems

2.1.1. Stress–strain relation for damage model
In the standard 1D damage model, the Hooke's law can be expressed as

$$\sigma = (1 - D)E\varepsilon \tag{1}$$

where σ, ε and E are the stress, strain and Young's modulus, respectively. Scalar variable D is called the damage variable that represents the degree of mechanical degradation and takes $0 \leqslant D \leqslant 1$. Here, zero means no damage, while 1 corresponds to complete fracture.

2.1.2. Relationship between cohesive force and crack opening displacement
Using an exponential function, we assume the following relationship in a 1D setting:

$$f = Ae^{-Bw} \tag{2}$$

where f is the cohesive force representing stress transfer on a fracture surface, w is the crack opening displacement (COD) of the fracture surface, and A and B are unknown material parameters.

Denoting the uniaxial tensile strength by f_t, we recognize f equals f_t when $w = 0$. Then, the parameter A can be expressed as

$$f_t = Ae^0 \rightarrow A = f_t \tag{3}$$

Also, the fracture energy, denoted by G_f, is defined as the energy per unit area required to form a fracture surface, which equals the area under the cohesive force-COD curve. According to this definition, the fracture energy must satisfy

$$G_f = \int_0^\infty f\,dw = A \int_0^\infty e^{-Bw}\,dw \tag{4}$$

so that unknown parameter B can be expressed as

$$G_f = \frac{A}{B} \rightarrow B = \frac{A}{G_f} = \frac{f_t}{G_f} \tag{5}$$

Consequently, the cohesive force-COD relationship for 1D problems can be expressed as

$$f = f_t e^{-\frac{f_t}{G_f}w} = f_t \exp\left(-\frac{f_t}{G_f}w\right) \tag{6}$$

2.1.3. Incorporation into damage model

The above-presented cohesive force-COD relationship involving the fracture energy is now incorporated into the conventional damage model. To do that, we first define the damage initiation strain, denoted by ε_0, which is related to the tensile strength, as

$$\varepsilon_0 = \frac{f_t}{E} \tag{7}$$

Supposing that a single element accommodates a single crack, COD w can be expressed as

$$w = \varepsilon h - \varepsilon_0 h = (\varepsilon - \varepsilon_0)h \tag{8}$$

where h is the length of an element in which the damage is evaluated, which corresponds to that of finite element in the finite element analysis. Here, the element length plays a role of converter of the strain measure to the measure of crack opening displacement and vice versa, since a finite element accommodates only the strain as an element variable.

In a damage model, cohesive force f on the fracture surface corresponds to stress σ as

$$f = \sigma \tag{9}$$

Substituting Eqs. (7)–(9) into Eq. (6), we can transform the cohesive force-COD relationship as

$$\sigma = E\varepsilon_0 \exp\left(-\frac{E\varepsilon_0 h}{G_f}(\varepsilon - \varepsilon_0)\right) \tag{10}$$

By converting this relationship into the same format as Eq. (1), we have

$$\sigma = \frac{\varepsilon_0}{\varepsilon} \exp\left(-\frac{E\varepsilon_0 h}{G_f}(\varepsilon - \varepsilon_0)\right) E\varepsilon = \left[1 - \left\{1 - \frac{\varepsilon_0}{\varepsilon} \exp\left(-\frac{E\varepsilon_0 h}{G_f}(\varepsilon - \varepsilon_0)\right)\right\}\right] E\varepsilon = [1 - D(\varepsilon)]E\varepsilon \tag{11}$$

Then, the damage variable can be represented as

$$D(\epsilon) = 1 - \frac{\epsilon_0}{\epsilon} \exp\left(-\frac{E\epsilon_0 h}{G_f}(\epsilon - \epsilon_0)\right) \tag{12}$$

where $\epsilon \geqslant 0$ is the maximum strain the material ever experienced.

Comparing the magnitudes of ε and ϵ, we can judge whether the current condition is loading or unloading such that

$$\begin{cases} \text{if } \epsilon \leqslant \varepsilon \to \epsilon = \varepsilon \ (\text{loading}) \\ \text{if } \epsilon > \varepsilon \to \epsilon = \epsilon \ (\text{unloading}) \end{cases} \tag{13}$$

Also, the judgment for damaged or undamaged states of the material is given as

$$\begin{cases} \text{if } \epsilon < \epsilon_0 \to D = 0 \ (\text{undamage}) \\ \text{if } \epsilon \geqslant \epsilon_0 \to D = D(\epsilon) \end{cases} \tag{14}$$

Within the framework of conventional continuum damage theory, the functional form of the damage variable is often given as [10,12–14]

$$D_{\text{ref}}(\epsilon) = 1 - \frac{\epsilon_0}{\epsilon}\left(1 - \alpha + \alpha e^{-\beta(\epsilon - \epsilon_0)}\right) \tag{15}$$

where α and β are the material parameters determined with reference to experimental results. Assuming $\alpha = 1$, we have

$$D_{\text{ref}}(\epsilon) = 1 - \frac{\epsilon_0}{\epsilon} e^{-\beta(\epsilon - \epsilon_0)} \tag{16}$$

Compared with Eq. (12), it is found that β is a parameter representing material toughness, as

$$\beta = \frac{E\epsilon_0 h}{G_f} \tag{17}$$

which involves the fracture energy G_f and the element length h resulting form Eq. (8). It is, therefore, recognized that the proposed model enables us to identify the parameters in Eq. (15) or Eq. (16) with those in fracture mechanics for concrete.

2.2. Extension to multi-dimensional problems

2.2.1. Equivalent strain

In an isotropic damage model for multi-dimensional problems, the damage nucleation and evolution law generally hinges on the definition of an equivalent strain, which can be used in place of the unidirectional strain ε in the 1D model presented above. Several definitions of equivalent strains have been suggested to describe the fractures of quasi-brittle materials; see for example, [26,27]. Among them, we employ the modified von-Mises model proposed by de Vree et al. [27], which has been

proven in a variety of studies on isotropic damage of concrete [10–14]. The equivalent strain ε_{eq} in the employed model is defined as

$$\varepsilon_{eq} = \frac{k-1}{2k(1-2v)}I_1 + \frac{1}{2k}\sqrt{\left(\frac{k-1}{1-2v}I_1\right)^2 + \frac{12k}{(1+v)^2}J_2} \tag{18}$$

where v and k represent the Poisson's ratio and the ratio of tensile and compressive strength, respectively. In the case of concrete, for example, $k \geqslant 10$ is suggested in general. Also, I_1 and J_2 are the first invariant of strain tensor $\boldsymbol{\varepsilon}$ and the second invariant of deviatoric strain tensor $\boldsymbol{e} = \boldsymbol{\varepsilon} - (1/3)\mathrm{tr}\,\boldsymbol{\varepsilon}$, which are respectively defined as

$$I_1 = \mathrm{tr}\,\boldsymbol{\varepsilon} = \varepsilon_{kk} \tag{19}$$

$$J_2 = \frac{1}{2}\boldsymbol{e} : \boldsymbol{e} = \frac{1}{2}e_{kl}e_{kl} \tag{20}$$

Fig. 1 shows some profiles of the equivalent strain on a 2D principal strain space with different values of tensile-compressive strength ratio k. The well-known characteristics of quasi-brittle materials like concrete, which shows low strength in tension and high strength in compression, is well demonstrated by k.

2.2.2. Damage model using equivalent strain

The direct extension of the Hooke's law in the 1D damage model, Eq. (1), to multi-dimensional problems can be given as

$$\boldsymbol{\sigma} = (1-D)\boldsymbol{c} : \boldsymbol{\varepsilon} \tag{21}$$

where $\boldsymbol{\sigma}$ and $\boldsymbol{c}$ are the Cauchy stress tensor and elastic modulus tensor, respectively. Since the damage variable here takes a scalar value, implying the lack of directionality, the model is commonly referred to as isotropic damage model.

Denoting the maximum equivalent strain in the deformation history by $\kappa \geqslant 0$, we recognize that the following functional form of the damage variable can be used for the isotropic damage model:

$$D(\kappa) = 1 - \frac{\kappa_0}{\kappa}\exp\left(-\frac{E\kappa_0 h_e}{G_f}(\kappa - \kappa_0)\right) \tag{22}$$

$$= 1 - \frac{\kappa_0}{\kappa}e^{-\beta(\kappa - \kappa_0)} \tag{23}$$

which is almost the same as that for the 1D model, given in Eq. (12), except that the representative element length h_e is adjusted for multi-dimensional problems as follows:

$$\text{Triangular element}: h_e = \sqrt{2A_e} \tag{24}$$

$$\text{Tetrahedral element}: h_e = (12V_e)^{1/3} \tag{25}$$

$$\text{Quadrilateral element}: h_e = \sqrt{A_e} \tag{26}$$

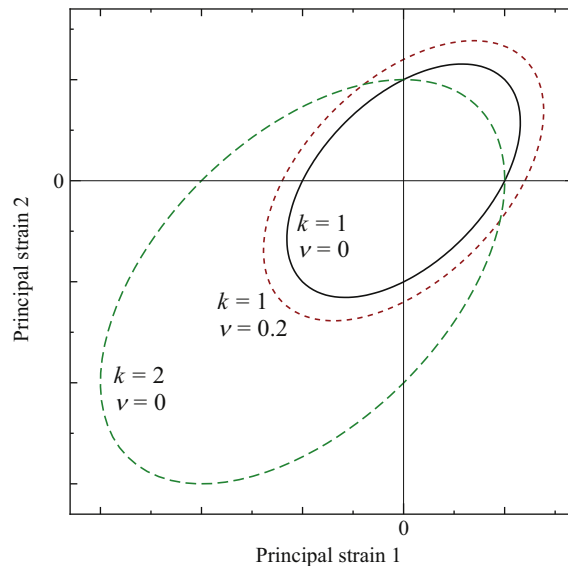$$\text{Hexahedral element}: h_e = V_e^{1/3} \tag{27}$$

Fig. 1. Contour plot of modified von-Mises equivalent strain.

Here, A_e and V_e are respectively the area of 2D elements and the volume of 3D elements. The multiplier 2 in Eq. (24) for triangular elements arises from the assumption that two triangles form a quadrilateral and the multiplier 12 in Eq. (25) for tetrahedral elements follows the same idea. Since a scalar parameter h_e is used as a representative element length to evaluate the damage of the element, the effect of direction of mesh division cannot be taken into account. Eqs. (13) and (14) apply for the multi-dimensional problems to judge whether loading or unloading, and whether damaged or undamaged, respectively.

2.2.3. Tangent modulus tensor – material Jacobian

When $\kappa < \kappa_0$ (before damage initiation or in elastic range), $D = 0$, and the material Jacobian $\boldsymbol{C}$ is expressed as

$$\boldsymbol{C} = \frac{\partial \boldsymbol{\sigma}}{\partial \boldsymbol{\varepsilon}} = \boldsymbol{c} \tag{28}$$

When $\kappa \geqslant \kappa_0$ and $\kappa \leqslant \varepsilon_{\text{eq}}$ (with damage and loading), $D = D(\kappa)$ and $\kappa = \varepsilon_{\text{eq}}$. Then, stress tensor $\boldsymbol{\sigma}$ and material Jacobian $\boldsymbol{C}$ are given as

$$\boldsymbol{\sigma} = (1 - D(\kappa))\boldsymbol{c} : \boldsymbol{\varepsilon} \tag{29}$$

$$\boldsymbol{C} = (1 - D(\kappa))\boldsymbol{c} - (\boldsymbol{c} : \boldsymbol{\varepsilon}) \otimes \frac{\partial D(\kappa)}{\partial \boldsymbol{\varepsilon}} \tag{30}$$

According to the chain rule of differentiation, $\partial D(\kappa)/\partial \boldsymbol{\varepsilon}$ can be expressed as

$$\frac{\partial D(\kappa)}{\partial \boldsymbol{\varepsilon}} = \frac{\partial D(\kappa)}{\partial \kappa} \frac{\partial \kappa}{\partial \varepsilon_{\text{eq}}} \frac{\partial \varepsilon_{\text{eq}}}{\partial \boldsymbol{\varepsilon}} \tag{31}$$

where the derivatives are evaluated as follows:

$$\frac{\partial D(\kappa)}{\partial \kappa} = \frac{\kappa_0}{\kappa} \left(\frac{1}{\kappa} + \beta \right) e^{-\beta(\kappa - \kappa_0)} \tag{32}$$

$$\frac{\partial \kappa}{\partial \varepsilon_{\text{eq}}} = 1 \tag{33}$$

$$\frac{\partial \varepsilon_{\text{eq}}}{\partial \boldsymbol{\varepsilon}} = \frac{a_1}{2k} \frac{\partial I_1}{\partial \boldsymbol{\varepsilon}} + \frac{1}{4k} \left(a_1^2 I_1^2 + a_2 J_2 \right)^{-\frac{1}{2}} \left(2a_1^2 I_1 \frac{\partial I_1}{\partial \boldsymbol{\varepsilon}} + a_2 \frac{\partial J_2}{\partial \boldsymbol{\varepsilon}} \right) \tag{34}$$

Here, we have defined a_1 and a_2 as

$$a_1 = \frac{k-1}{1-2v}, \quad a_2 = \frac{12k}{(1+v)^2} \tag{35}$$

When $\kappa \geqslant \kappa_0$ and $\kappa \geqslant \varepsilon_{\text{eq}}$ (with damage and unloading), the effect of damage is present, but the damage never propagates. Then, κ is not updated as $\kappa = \kappa$ so that Eq. (31) yields

$$\frac{\partial D(\kappa)}{\partial \boldsymbol{\varepsilon}} = \frac{\partial D(\kappa)}{\partial \kappa} \cdot 0 \cdot \frac{\partial \varepsilon_{\text{eq}}}{\partial \boldsymbol{\varepsilon}} = \boldsymbol{0} \tag{36}$$

Consequently, the material Jacobian $\boldsymbol{C}$ becomes

$$\boldsymbol{C} = (1 - D(\kappa))\boldsymbol{c} \tag{37}$$

In numerical analyses with the proposed model, the implicit solution procedure based on the standard Newton–Raphson (NR) method is employed. If the convergent solution is not obtained due to the numerical instability especially in the softening regime, we return to the initial iteration step of the incremental process and apply the modified NR method instead.

3. Performance demonstrations

Several numerical examples are presented to verify the capability of the model for evaluating the fracture process with high accuracy and to demonstrate its performance for providing mesh-independent solutions.

3.1. Fracture under uniaxial tension

A numerical examination is conducted to verify the basic characteristics of the proposed damage model for uniaxial tensile fractures. Fig. 2 shows the analysis targets along with meshes, which are prepared so as to have damage only in the elements aligned in their center. Four-types of 2D and 3D finite element (FE) meshes of different linear elements are prepared to examine the element lengths given in Eqs. (24)–(27); they are standard triangular (T3), quadrilateral (Q4), tetrahedral (T4) and hexahedral elements (H8). Here, the term "standard" to explain elements implies throughout this study that these elements are not endowed with special techniques such as reduced integrations and introduction of incompatible modes. Material parameters are provided in the figure, and the Poisson's ratio is set at zero to prevent the Poisson effect.
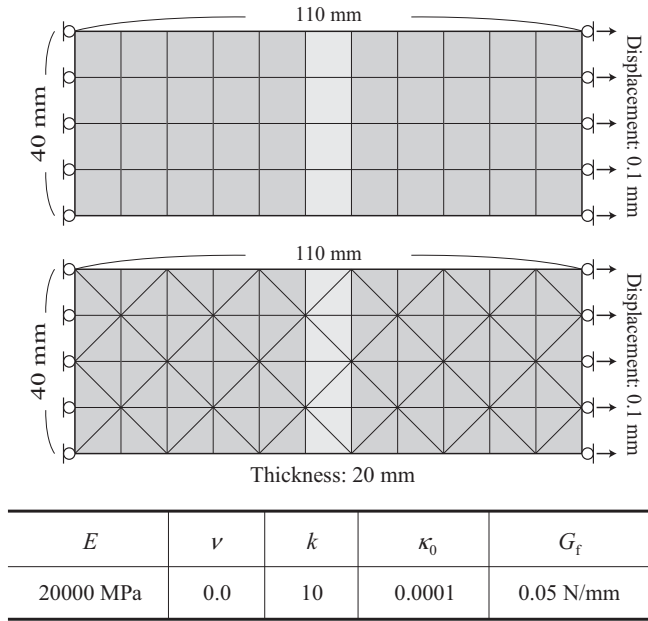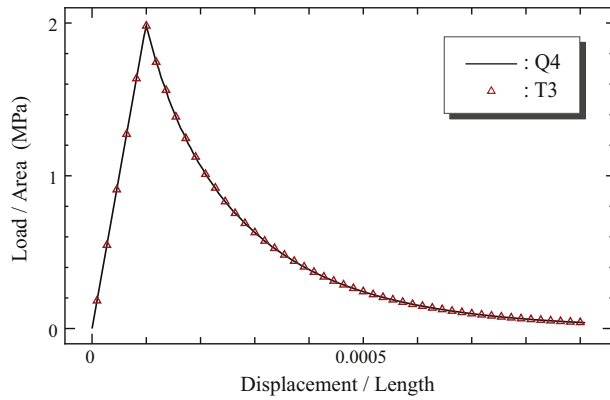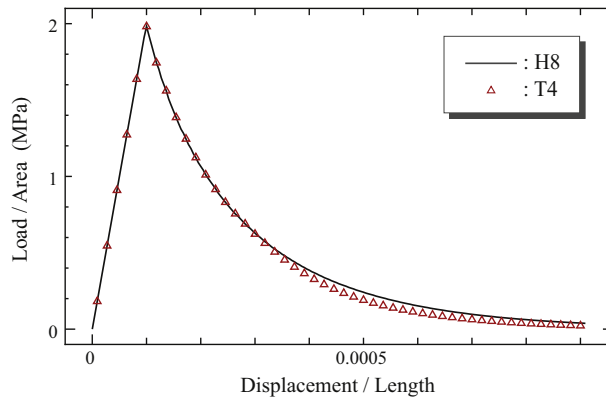
E	ν	k	κ_0	G_f
20000 MPa	0.0	10	0.0001	0.05 N/mm

Fig. 2. Uniaxial tensile fracture problem.

(a) Load-displacement curves in 2-D simulation

(b) Load-displacement curves in 3-D simulation
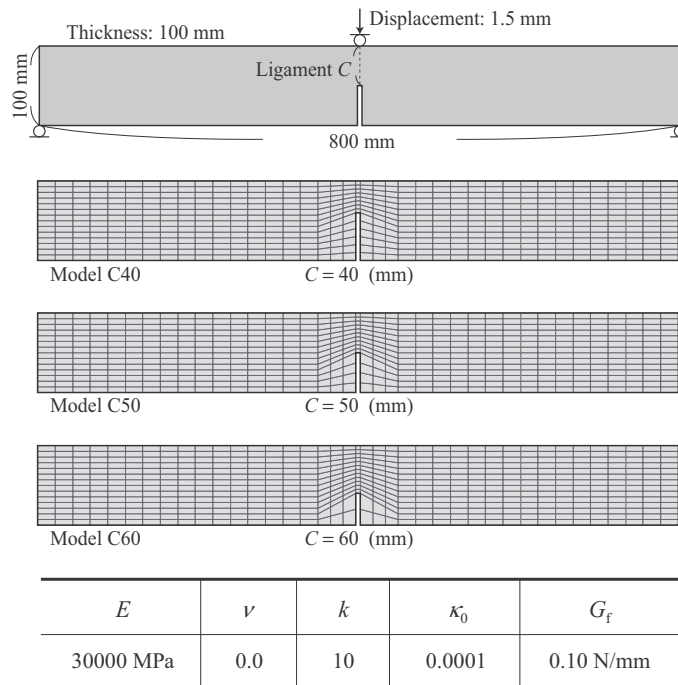
Fig. 3. Load versus displacement in uniaxial problem.

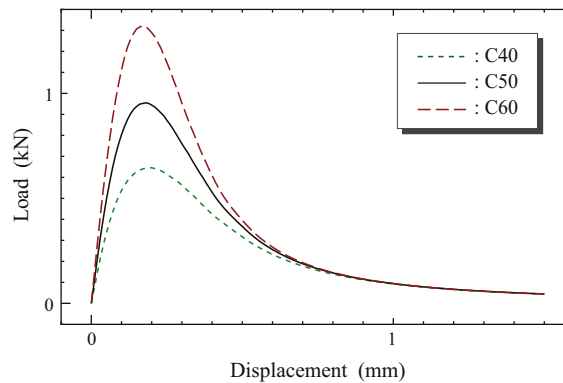Fig. 4. Three-point bending test on beam with a differently-sized single-edge notch.

E	ν	k	κ_0	G_f
30000 MPa	0.0	10	0.0001	0.10 N/mm

Fig. 5. Load versus displacement in 3-point bending problem.

Fig. 3 shows the load–displacement curves obtained by the 2D and 3D simulations with different FE meshes. In the figure, the ordinate and abscissa represent the apparent stress and strain, respectively. As can be seen from these curves, the results obtained are almost the same for all the element types. Although the results of the tetrahedral elements are slightly different from that of the hexahedral elements, a source of error seems to be the assumption about element length that 12 tetrahedrons form a hexahedron; see Eq. (25).

3.2. Fracture in beams with a notch under three-point bending

Fracture energy, which is one of the representative fracture mechanics parameters for concrete, is defined as the energy per unit area required to form a fracture surface or the energy dissipated when the fracture surface of a unit area is formed. In this context, Li et al. [28] have proposed a method of evaluating the fracture energy of concrete by using the J-integral. In the method, three-point bending tests are performed on beam specimens with different notch lengths, and then the differences in dissipated energy and in notch length enable us to estimate the fracture energy. Here, following this idea, we conduct numerical examination to evaluate the fracture energy and discuss the energy characteristics of the proposed damage model.

3.2.1. Analysis target and conditions

The analysis target is the beam with a notch subjected to three-point bending as shown in Fig. 4, in accordance with the RILEM method [29]. We prepare three FE models with the same span, height and thickness, but different notch lengths. The finite elements used here are the standard bilinear quadrilateral elements. Setting the material parameters as provided in the figure, we conduct crack propagation analyses under displacement control.

3.2.2. Analysis results and discussion

Fig. 5 shows the load–displacement curves obtained by the numerical analyses with the proposed model. By calculating the area under these curves, we obtain the total energy dissipated in the fracture process in each model, which corresponds to the energy necessary to form the total area of fracture surface in the three-point bending test. Here, the difference in total dissipated energy between two separate models corresponds to the difference in total area of fracture surface. Therefore, the fracture energy, namely the energy dissipation per unit area, can be evaluated by dividing this difference in total dissipated energy by the difference in area of fracture surface.

For example, denoting the difference in dissipated energy between Model C50 and C40 by ΔU_{50-40} and the difference in height minus notch length times thickness by $\Delta A (= 10 \times 100 \text{ mm}^2)$, we can calculate the apparent fracture energy as $G_F = \Delta U / \Delta A$, which can be compared with the fracture energy G_f set as a material parameter in our numerical analyses.

The apparent fracture energy G_F^{50-40} obtained from Model C50 and C40, and the apparent fracture energy G_F^{60-50} obtained from Model C60 and C50, are respectively calculated as follows:

$$G_F^{50-40} = \frac{4.57500 \times 10^2 - 3.5802 \times 10^2}{(50 - 40) \times 100} = 0.09948 \cdots \approx 0.1 \text{ N/mm}$$

$$G_F^{60-50} = \frac{5.57980 \times 10^2 - 4.57500 \times 10^2}{(60 - 50) \times 100} = 0.10048 \cdots \approx 0.1 \text{ N/mm}$$

Here, the apparent fracture energies G_F^{50-40} and G_F^{60-50}, estimated from the numerical analyses, reproduce the material parameter $G_f = 0.1$ N/mm with satisfactory accuracy. This result confirms that the simulated crack behavior with strain-softening meets the definition of fracture energy. Therefore, the proposed damage model enables us to perform crack propagation analyses in consistency with fracture mechanics for concrete.

3.3. Flexural fracture in arch-shaped structure

The proposed damage model contains the ratio of tensile and compressive strength denoted by k as shown in Eq. (18), which enables us to simulate the fracture behavior of concrete such that the compressive strength is higher than the tensile one. We here examine an arch-shaped structure subjected to bending moment for the effect of the ratio in the damage model on the fracture behavior.
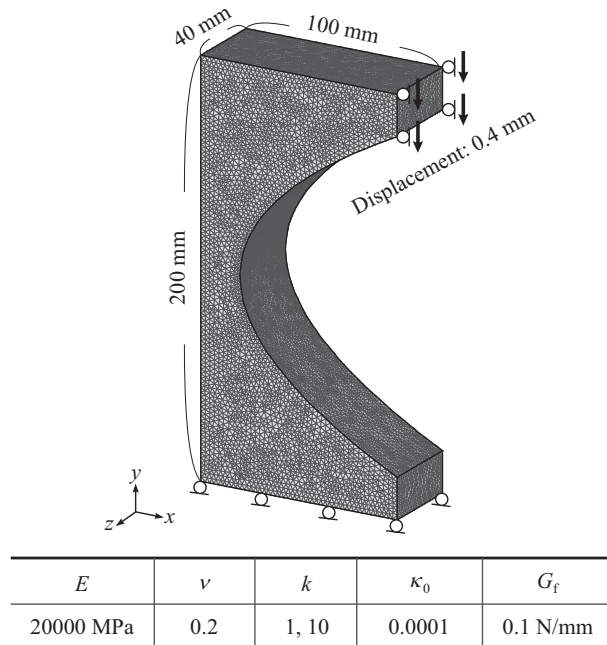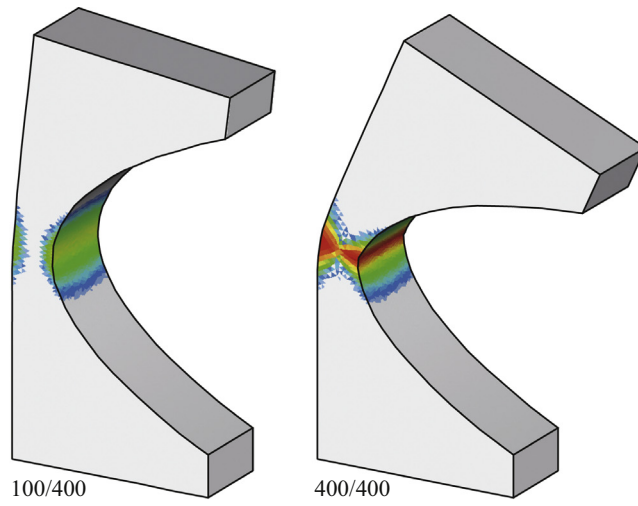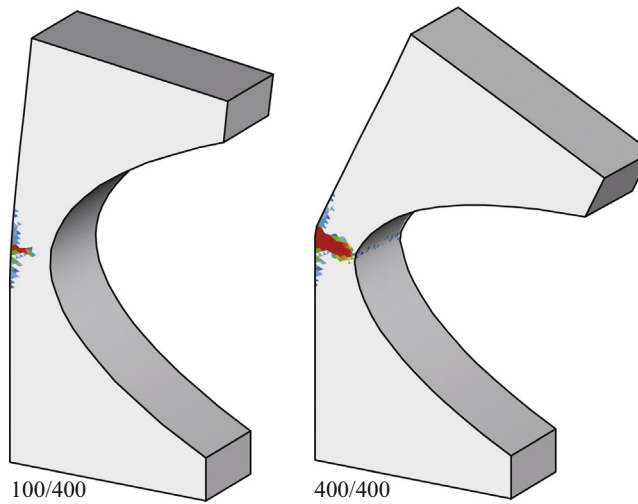

E	ν	k	κ_0	G_f
20000 MPa	0.2	1, 10	0.0001	0.1 N/mm

Fig. 6. Fluxural fracture problem of arch-shaped model.

100/400　　　　　　　　400/400

(a) Damage distribution ($k = 1$)

100/400　　　　　　　　400/400

(b) Damage distribution ($k = 10$)

0.0 ▭ 1.0

Fig. 7. Propagation of damage in arch-shaped model.
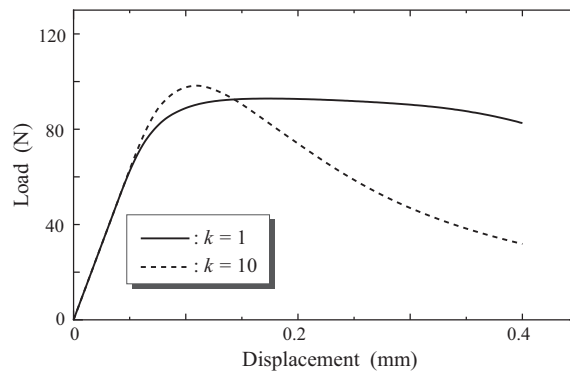
Fig. 8. Load versus displacement in arch-shaped model.

Displacement: 0.05 mm

Model H1

100 mm

Displacement: 0.1 mm

Displacement: 0.1 mm

200 mm

200 mm

Model H2

Model H3

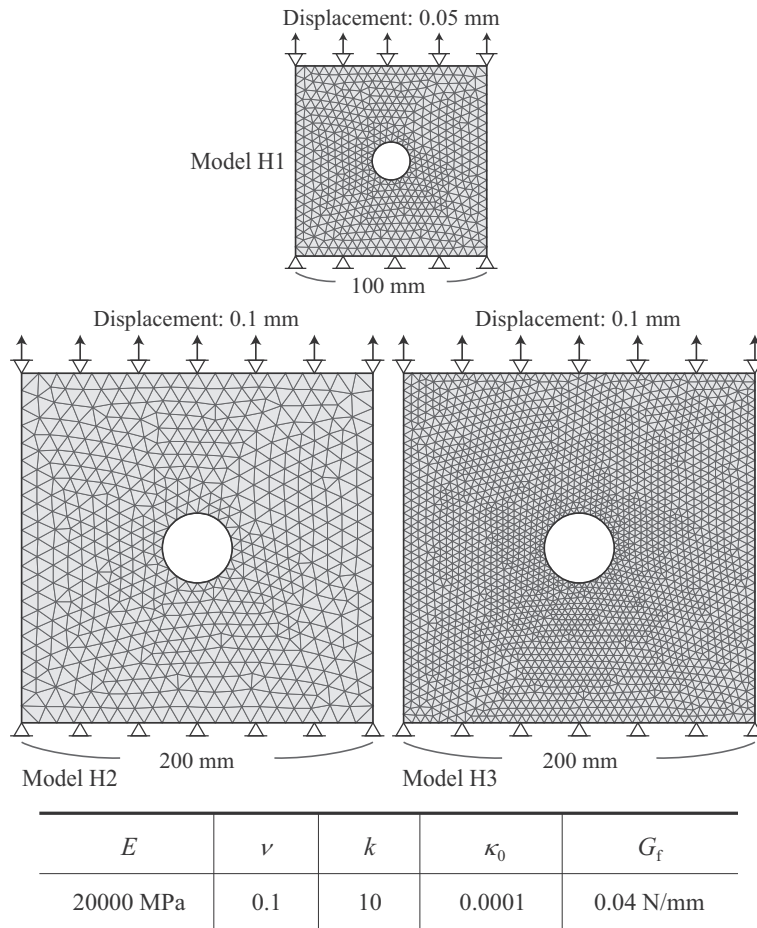| E	ν	k	κ_0	G_f
20000 MPa	0.1	10	0.0001	0.04 N/mm

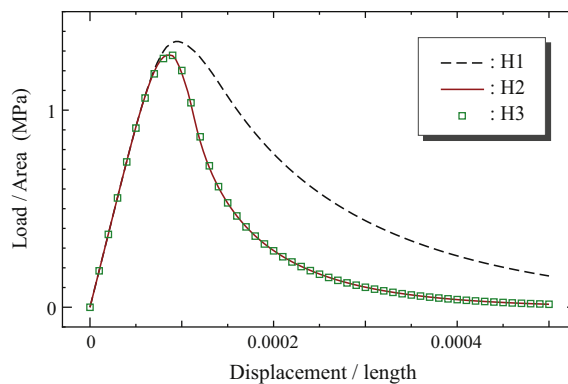**Fig. 9.** Tensile fracture problem of differently-sized plate with a circular hole.
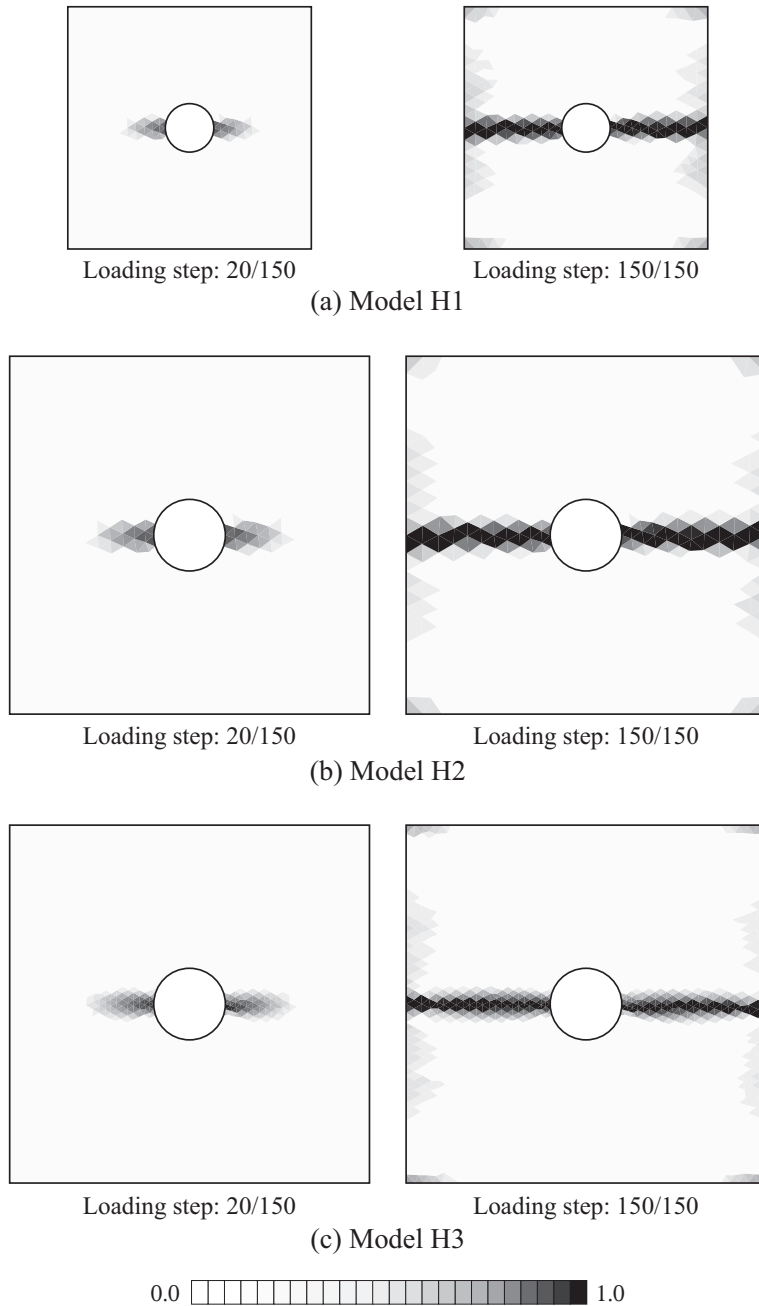

Fig. 10. Load versus displacement in circular hole problem.

The analysis target is the arch-shaped structure under the boundary condition giving rise to bending moment as shown in Fig. 6. The standard linear tetrahedral elements are used to prepare the FE model. The material prameters set in this example are shown in the same figure. Crack propagation analyses are carried out under displacement control by varying the ratio of tensile and compressive strength.

Fig. 7 shows the distribution of damage for the two analysis cases. In case of $k = 1$, damages start from both the tensile and compressive sides of the arch-shaped structure. This is because the compressive strength is the same as the tensile one. In contrast, as can be seen from the case of $k = 10$, the damage arises only from the tensile side due to the condition that the

Loading step: 20/150   Loading step: 150/150

(a) Model H1

Loading step: 20/150   Loading step: 150/150

(b) Model H2

Loading step: 20/150   Loading step: 150/150

(c) Model H3

0.0 ▯▯▯▯▯▯▯▯▯▯▯▯▯▯▯▯▯▯▯▮▮▮ 1.0

Fig. 11. Propagation of damage in circular hole problem.

compressive strength is ten times higher than the tensile one. Therefore, setting the ratio of strength to a large value makes it possible to simulate realistic crack propagations as observed in concrete.

Fig. 8 shows the load–displacement curves for the two analysis cases. As can be seen from the figure, the responses are different. The results show that the ratio of strength has influences on not only crack propagations but also apparent load–displacement responses.

3.4. Capability for mesh independency

It is known that damage models without any special treatment suffers from the strong mesh dependency in simulating fractures involving strain-softening behavior [15,27]. In this section, using the proposed model, we perform a case study of fracture simulations to demonstrate its capability for mesh-independency.

The analysis target is a plate with a circular hole. For the case study, we prepare three kinds of FE meshes as shown in Fig. 9. Model H1 is set for reference. Also, Model H2 is prepared to be double the mesh size and the model size of H1, and H3 has the same mesh size as H1 with double the model size of H1. Standard linear triangular elements are randomly arranged to form the meshes. The material parameters used in the case study are provided in the figure, and the plane strain conditions are assumed in the finite element analyses.

Fig. 10 shows the load–displacement curves for the three analysis cases. The ordinate indicates the apparent stress that is defined as the load divided by the loading area, while the abscissa represents the apparent strain that is the displacement divided by the height of the model. As can be seen from the results, the responses of Model H2 and Model H3, which are the same in model size but different in mesh size, are almost the same. These results thus confirmed that the fracture analysis with the proposed model do not depend on mesh size. On the other hand, comparing the results of H1 and H2 (or H3), which are different in model size, we can see that Model H2 (or H3) with a larger model size exhibits rather brittle response. This type of dependency of the strain-softening responses on the model size – a well-known characteristic of fracture behavior – has been reproduced by the application of the proposed damage model.

Fig. 11 shows the damage evolution for all the cases. Here, the values $D = 0$ and $D = 1$ are colored in white and black, respectively, and the gray scale is the intermediate value of D. Again, it is found that the locations and distribution properties of the damage variable do not depend on the mesh size, when the results of Model H2 and H3 are compared. From the results and discussions here, we can confirm that failure simulations with the proposed model, which satisfies the energy balance in terms of the fracture energy, reflect the effect of model size without dependency on the mesh size.

4. A benchmark problem for mixed-mode fracture

Taking a benchmark problem for mixed-mode fracture as the final numerical example, we carry out the crack propagation analysis with the proposed damage model, to verify the reproducibility of the experimental result.

4.1. Nooru-Mohamed test

The experiments conducted by Nooru-Mohamed [30], in which tensile (Mode I) and shear (Mode II) loads are applied to a mortar specimen, are often referred as benchmark problems for mixed-mode fracture in concrete or other quasi-brittle materials, and their results have widely be utilized to validate the numerical results obtained by various techniques for fracture simulations [11,31–34].

Fig. 12 shows a schematic of the rectangular parallelepiped specimen along with the boundary conditions and the representative crack paths obtained in one of the experiments. Here, the solid and dotted curves are the crack paths observed on the front and reverse sides of the specimen. Two notches are introduced to the specimen, which is sometimes called DENS (Double Edge Notched Specimen). Stiff plates (T, B, L, R in the figure) are attached to the four sides of the specimen to apply
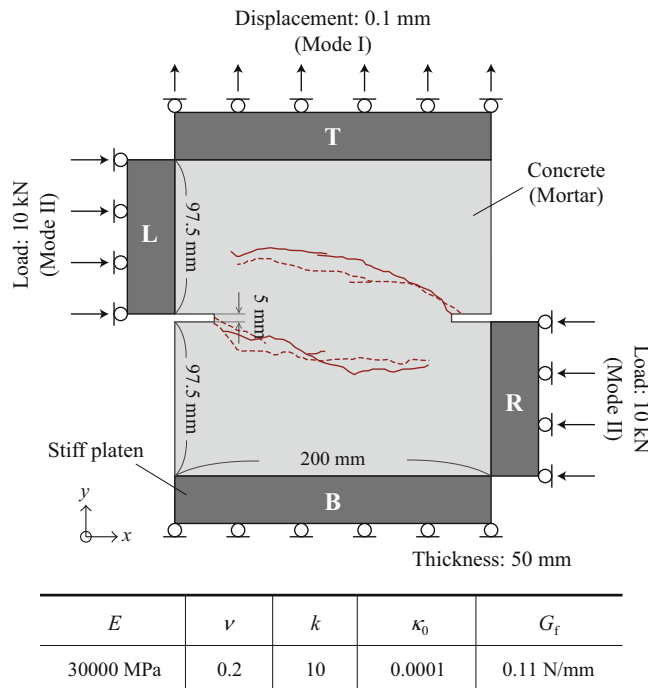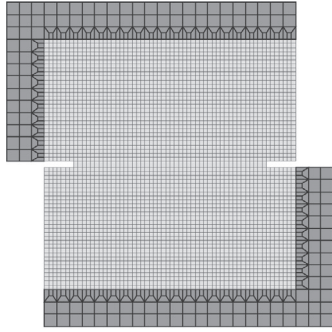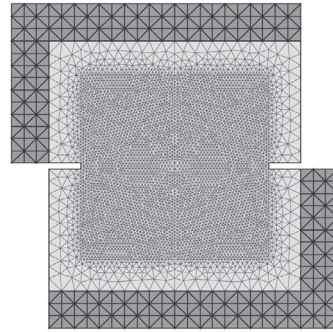

E	ν	k	κ_0	G_f
30000 MPa	0.2	10	0.0001	0.11 N/mm

Fig. 12. Nooru-Mohamed problem.

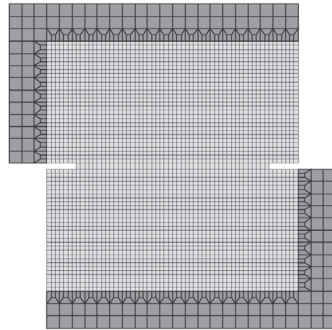4,112 nodes, 4,024 elements   5119 nodes, 10,112 element
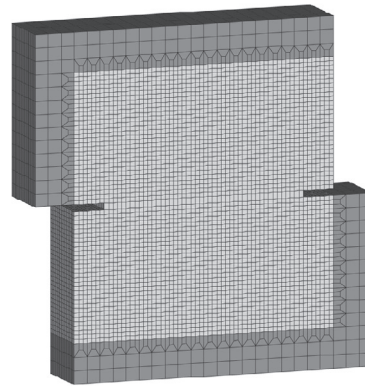
(a) 2D mesh with quadrilateral elements   (b) 2D mesh with triangular elements

65,792 nodes, 60,360 elements
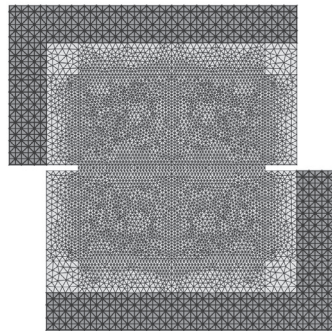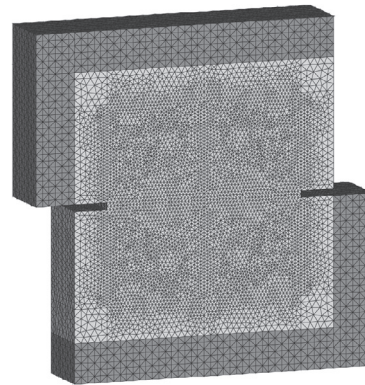
Front view   3D view

(c) 3D mesh with hexahedral elements

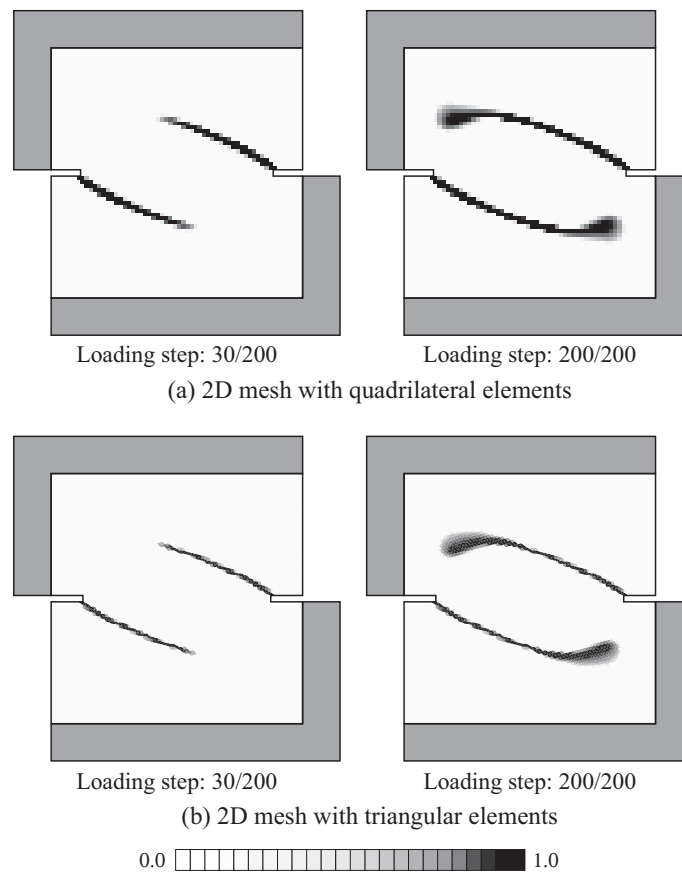112,413 nodes, 625,252 elements

Front view   3D view

(d) 3D mesh with tetrahedral elements

Fig. 13. Finite element mesh for Nooru-Mohamed problem.

the loading. With plates L and R being fixed and kept upright, the constant horizontal pressure is applied to both of the plates from the beginning to the end, and the displacement is incrementally given to plate T in the vertical direction. Although the experiments were conducted with different values of horizontal pressure, we here employ only the case of applied horizontal load of 10 kN.

4.2. Analysis conditions

As shown in Fig. 13, the FE meshes with four different element types in 2D and 3D are used for fracture simulations for the Nooru-Mohamed problem. One of the 2D meshes is generated with standard four-node quadrilateral elements and the other is with standard three-node triangular elements. The 3D meshes are generated with standard eight-node hexahedral and

Loading step: 30/200　　　　　　Loading step: 200/200

(a) 2D mesh with quadrilateral elements

Loading step: 30/200　　　　　　Loading step: 200/200

(b) 2D mesh with triangular elements

0.0 ▯▯▯▯▯▯▯▯▯▯▯▯▯▯▯▯▯▯▯ 1.0

Fig. 14. Propagation of damage in Nooru-Mohamed problem: 2D results.

four-node tetrahedral elements. Bilateral and diphycercal symmetries are kept in these meshes. The stiff plates in each mesh are also generated with the same type of elements with that of the mortar, and are connected to the mortar domain. The material parameters used in the numerical analyses are provided in the figure, and the Young's modulus of the stiff plates is set to 100 times that of the mortar specimen. 2D analyses are carried out under the plane strain conditions.

With the y-component of the displacement on the lower surface of plate B being set at zero, constant horizontal loads of 10 kN are applied to the left-end of plate L and the right-end of plate R from the beginning to the end, while the forced displacement only in the y-direction is incrementally applied on the upper surface of plate T. Expecting mirror-symmetric deformations, we impose no constraints of the x-component of displacement on all the plates' edges. Although the detachment of the mortar part from the stiff plates might be possible in actual experiments, we do not consider such imperfect situations in this study.

4.3. Analysis results and discussion

Figs. 14 and 15 show the distributions of damage variables at two stages of evolutions, which approximately represent crack paths, along with the experimental ones. Here, the meanings of white and black colors are the same as before. With reference to Fig. 12, the numerical analyses with the proposed damage model provided very similar results to the experimentally obtained crack paths. It should be emphasized that the fracture nucleation and propagation in the numerical analyses are determined only by the tensile strength in terms of the equivalent strain of the modified von-Mises model, which involves the elastic properties and the ratio of tensile and compressive strength. In other words, the numerical results with the proposed damage model reproduced the mixed-mode fracture characteristics similar to the experimental result, even though Mode I and Mode II fractures are not distinguished in the material model.

Fig. 16 shows the obtained load–displacement curves along with the two experimental results provided in the [30]. For reference, the result of the X-FEM analysis with the same set of material parameters as the present analysis, which is reported in [33], is also provided in the figure. As can be seen from these curves, the analysis results with the proposed model are comparable with the experimental ones. More specifically, the softening responses of the numerical results are conformable with the experimental ones. However, when the numerical results are mutually compared, they are moderately different especially in the softening behavior after the peak loads.
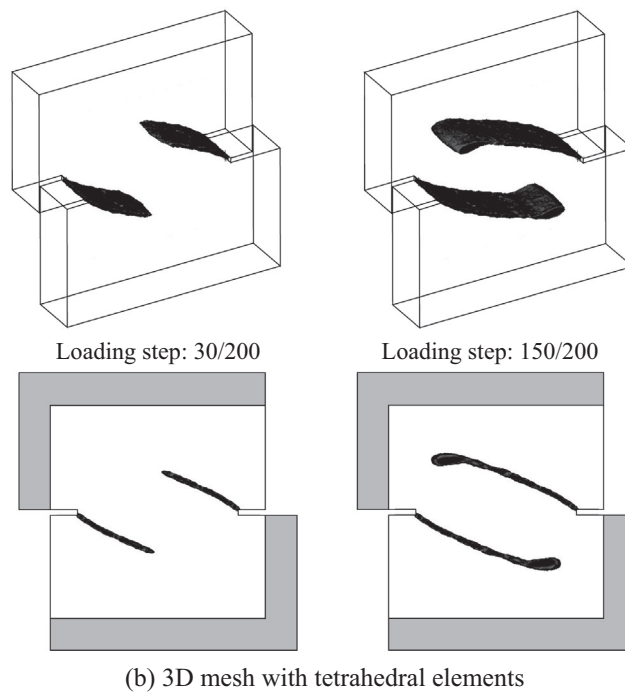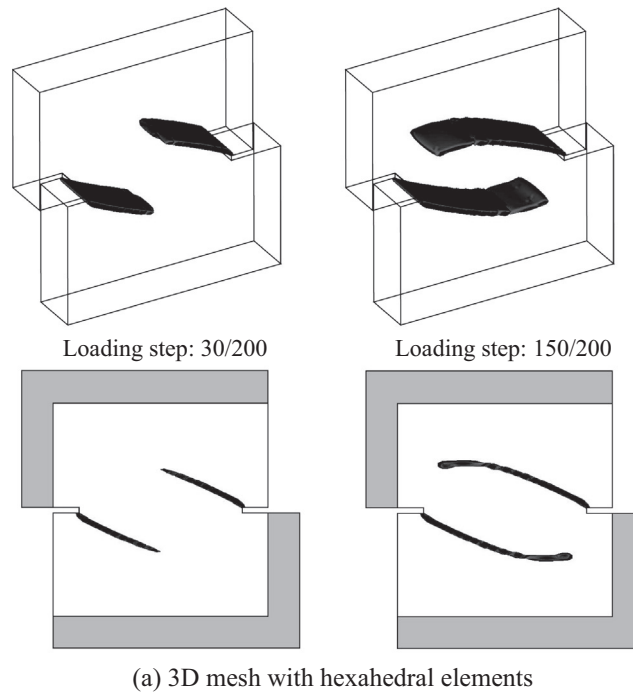
Loading step: 30/200   Loading step: 150/200

(a) 3D mesh with hexahedral elements

Loading step: 30/200   Loading step: 150/200

(b) 3D mesh with tetrahedral elements

Fig. 15. Propagation of damage in Nooru-Mohamed problem: 3D results.

When the 2D results with quadrilateral and triangular elements are compared, the triangular mesh provides more brittle behavior than the structured mesh with quadrilateral elements. Also, the results of the latter model, namely those of the structured mesh with quadrilateral elements, exhibit zigzag crack paths in an oblique direction, as can be observed in Fig. 14. Furthermore, the crack paths obtained with triangular elements seem to be narrower than those with quadrilateral elements. The difference in softening behavior or brittleness between the results with triangular and quadrilateral elements
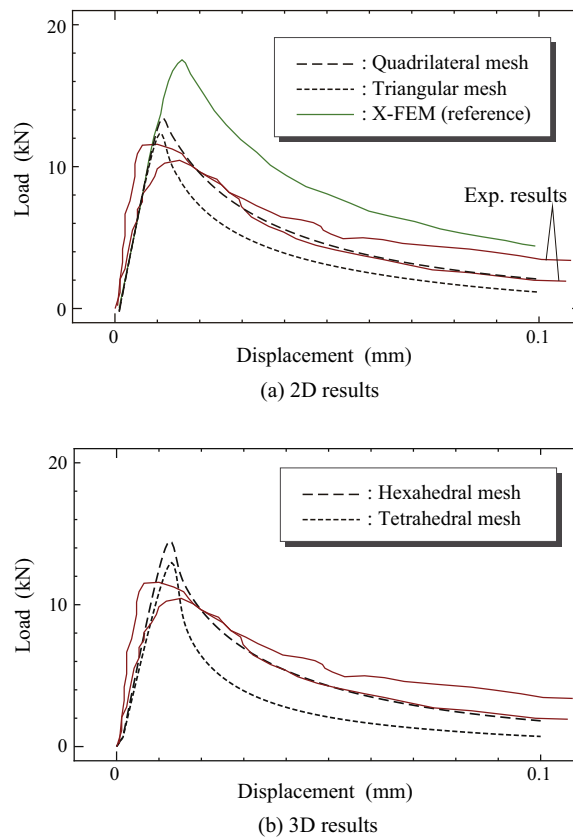
(a) 2D results

(b) 3D results

Fig. 16. Load versus displacement in Nooru-Mohamed problem.

implies that the softening behavior characterized with the proposed model may be slightly affected by element types and mesh topologies especially for non-linear crack paths. As can be seen from Fig. 16, the same tendency of softening behavior is observed for the 3D results with hexahedral and tetrahedral elements, though the difference in crack paths is not significant in comparison with the 2D results.

The final remark is addressed on the effect of Poisson's ratio. Since the present study employs the equivalent strain based on the modified von-Mises model for the fracture criteria, the value of the Poisson's ratio affects both shear and volumetric deformations especially for 2D analyses under the plane strain condition. Although the results in this example problem are obtained with Poisson's ratio of 0.2, we have confirmed that the smaller the value of Poisson's ratio, the larger the peak strength in 2D analyses. Moreover, we have also confirmed that the load–displacement curve coincides with that of the X-FEM provided in Fig. 16 as a reference solution, if the Poisson's ratio is set at 0.0 in 2D analysis under the plane strain condition.

5. Conclusion

To avoid mesh-size dependency, most of the previous studies using damage models employ nonlocal models such as the integral average model and the gradient model, which require parameters whose physical interpretation is ambiguous. The nonlocal parameters in such damage models are associated with the profile of material's distribution, but not with material properties in fracture mechanics, to define the damage evolution law.

In this paper, without using any conventional nonlocal model of such as those with integral average or gradient, we proposed an isotropic damage model to characterize the strain-softening behavior within the framework of fracture mechanics for concrete. After presenting the formulation in 1D problems by incorporating the cohesive force-COD relationship of concrete into the damage model in terms of the fracture energy, we extended it to multi-dimensional problems using the equivalent strain based on the modified von-Mises model. A series of crack propagation analyses has been conducted to verify the validity of the proposed model and to demonstrate its performance and capability in simulating mesh-independent fracture responses involving the strain-softening behavior and in reproducing experimentally reported crack paths under the mixed-mode loading.

While our focus has been placed on the fracture processes mainly caused by locally tensile cracking, the applicability of the proposed model to fracture phenomena under compressive loading has to be examined in the near future. Also, the investigation of the effects of heterogeneities on the fracture behavior of concrete is an important subject of study.

Acknowledgements

References

[1] Jirásek M. Comparative study on finite elements with embedded discontinuities. Comput Methods Appl Mech Engng 2000;188:307–30.
[2] Moës N, Dolbow J, Belytschko T. A finite element method for crack growth without remeshing. Int J Numer Meth Engng 1999;46:131–50.
[3] Terada K, Asai M, Yamagishi M. Finite cover method for linear and nonlinear analyses of heterogeneous solids. Int J Numer Meth Engng 2003;58:1321–46.
[4] Wells GN, Sluys LJ. Application of embedded discontinuities for softening solids. Engng Fract Mech 2000;65:263–81.
[5] Kurumatani M, Terada K. Finite cover method with multi-cover-layers for the analysis of evolving discontinuities in heterogeneous media. Int J Numer Meth Engng 2009;79:1–24.
[6] Bažant ZP, Oh BH. Crack band theory for fracture of concrete. Mater Struct 1983;16:155–77.
[7] Jirásek M, Zimmermannl T. Analysis of rotating crack model. J Engng Mech 1998;124:842–51.
[8] Jirásek M, Zimmermann T. Rotating crack model with transition to scalar damage. J Engng Mech 1998;124:277–84.
[9] Bažant ZP, Ožbolt J. Nonlocal microplane model for fracture, damage and size effect in structures. J Engng Mech 1990;116:2485–505.
[10] Geers MGD, de Borst R, Peerlings RHJ. Damage and crack modeling in single-edge and double-edge notched concrete beams. Engng Fract Mech 2000;65:247–61.
[11] Jirásek M, Grassl P. Evaluation of directional mesh bias in concrete fracture simulations using continuum damage models. Engng Fract Mech 2008;75:1921–43.
[12] Peerlings RHJ, de Borst R, Brekelmans WAM, Geers MGD. Gradient-enhanced damage modelling of concrete fracture. Mech Cohes-Frict Mater 1998;3:323–42.
[13] Rodríguez-Ferran A, Bennett T, Askes H, Tamayo-Mas E. A general framework for softening regularisation based on gradient elasticity. Int J Solids Struct 2011;48:1382–94.
[14] Giry C, Dufour F, Mazars J. Stress-based nonlocal damage model. Int J Solids Struct 2011;48:3431–43.
[15] Pijaudier-Cabot G, Bažant ZP. Nonlocal damage theory. J Engng Mech 1987;113:1512–33.
[16] Bažant ZP, Pijaudier-Cabot G. Nonlocal damage, localization instability and convergence. J Appl Mech 1988;55:287–93.
[17] Peerlings RHJ, de Borst R, Brekelmans WAM, de Vree JHP. Gradient enhanced damage for quasi-brittle materials. Int J Numer Meth Engng 1996;39:3391–403.
[18] Bažant ZP, Pijaudier-Cabot G. Measurement of characteristic length of nonlocal continuum. J Engng Mech 1989;115:755–67.
[19] Kuhl E, Ramm E, de Borst R. An anisotropic gradient damage model for quasi-brittle materials. Comput Methods Appl Mech Engng 2000;183:87–103.
[20] Hillerborg A, Modéer M, Petersson PE. Analysis of crack formation and crack growth in concrete by means of fracture mechanics and finite elements. Cem Concr Res 1976;6:773–82.
[21] Moës N, Belytschko T. Extended finite element method for cohesive crack growth. Engng Fract Mech 2002;69:813–33.
[22] Gasser TC, Holzapfel GA. Modeling 3D crack propagation in unreinforced concrete using PUFEM. Comput Methods Appl Mech Engng 2005;194:2859–96.
[23] Terada K, Ishii T, Kyoya T, Kishino Y. Finite cover method for progressive failure with cohesive zone fracture in heterogeneous solids and structures. Comput Mech 2007;39:191–210.
[24] Wells GN, Sluys LJ. A new method for modelling cohesive cracks using finite elements. Int J Numer Meth Engng 2001;50:2667–82.
[25] Mergheim J, Kuhl E, Steinmann P. A finite element method for the computational modelling of cohesive cracks. Int J Numer Meth Engng 2005;63:276–89.
[26] Mazars J. A description of micro- and macroscale damage of concrete structures. Engng Fract Mech 1986;25:729–37.
[27] de Vree JHP, Brekelmans WAM, van Gils MAJ. Comparison of nonlocal approaches in continuum damage mechanics. Comput Struct 1995;55:581–8.
[28] Li VC, Chan CM, Leung CKY. Experimental determination of the tension-softening relations for cementitious composites. Cem Concr Res 1987;17:441–52.
[29] RILEM Draft Recommendation (50-FMC). Determination of the fracture energy of mortar and concrete by means of three-point bend tests on notched beams. Mater Struct 1985;18:285–90.
[30] Nooru-Mohamed MB. Mixed-mode fracture of concrete: an experimental approach. Ph.D. Thesis, Technische Universiteit Delft; 1992.
[31] di Prisco M, Ferrara L, Meftah F, Pamin J, de Borst R, Mazars J, et al. Mixed mode fracture in plain and reinforced concrete: some results on benchmark tests. Int J Fract 2000;103:127–48.
[32] Cervera M, Chiumenti M. Smeared crack approach: back to the original track. Int J Numer Anal Meth Geomech 2006;30:1173–99.
[33] Dumstorff P, Meschke G. Crack propagation criteria in the framework of X-FEM-based structural analyses. Int J Numer Anal Meth Geomech 2007;31:239–59.
[34] Al-Rub RKA, Kim S-M. Computational applications of a coupled plasticity-damage constitutive model for simulating plain concrete fracture. Engng Fract Mech 2010;77:1577–603.